Fluid Composition, Thermal Conditions, Fluid-structural Relationships and Graphite Alteration of the Phoenix Uranium Deposit, Athabasca Basin, Saskatchewan

Kewen Wang[1], Guoxiang Chi[1], Kathryn M. Bethune[1], and Colin D. Card[2]

1. *Geology Department, University of Regina, 3737 Wascana Parkway, Regina, Saskatchewan, S4S 0A2*
2. *Saskatchewan Geological Survey, Regina, 2101 Scarth Street, Regina, Saskatchewan, S4P 2H9*

Abstract

The Phoenix deposit is a high-grade unconformity-related uranium deposit located in the southeastern Athabasca Basin. Previous studies have revealed similar features to other well-known unconformity-related uranium deposits in the region, but the composition and thermal conditions of the mineralization fluids, the hydrodynamic relationship between structures and fluid pressure, and the nature of graphite degradation near mineralization zones remain unclear. Field (drill core) investigations, petrographic studies of altered and mineralized host rocks, and microthermometric and microstructural studies of fluid inclusions indicate that different structural regimes and fluid systems were developed in the pre-Athabasca stage versus the syn- to post-Athabasca, uranium mineralization stage. The pre-Athabasca stage was characterized by ductile deformation and circulation of metamorphic fluids in a relatively high *P–T* environment, whereas the syn- to post-Athabasca mineralization stage was characterized by brittle deformation and circulation of basinal brines in a relatively low *P–T* environment (with fluid inclusion homogenization temperatures of 80 to 135 °C), in which the fluid may have experienced boiling, as indicated by the coexistence of vapour-only and biphase aqueous inclusions. Preliminary fluid inclusion plane (FIP) orientation studies reveal the dominance of subvertical microfractures in cross-cutting quartz veins in the basement, possibly indicating an extensional regime during certain periods of time in the syn- to post-Athabasca mineralization stage. Preliminary petrographic and Raman spectroscopic studies of graphite suggest that the crystal structure of the graphite tends to be more disordered toward the mineralized zones, which may potentially be used as an indicator of mineralization.

Introduction

The Phoenix uranium deposit is located 35 km southwest of the world-class McArthur River uranium deposit in the southeastern Athabasca Basin (Fig. 1). It consists of a series of high-grade unconformity-related uranium zones associated with a NE-trending, moderately SE-dipping reverse fault, the WS shear zone. Previous geological and geochemical studies have revealed features similar to other unconformity-related uranium deposits in the region (e.g. Gamelin et al., 2010; Kerr, 2010; Power et al., 2012; Dann et al., 2014), but the composition, temperature and pressure of the fluids associated with mineralization have not yet been investigated by fluid inclusion techniques. In addition, like other well-studied unconformity-related uranium deposits, the structural controls on mineralization, particularly the hydrodynamic relationship between structures (and related stresses) and fluid pressure, are not well understood. Furthermore, the prevalence of graphite in metapelite in basement rocks at the Phoenix deposit provides an opportunity to explore potential roles of graphite in the formation of unconformity-related uranium deposits, given the known spatial association between graphite and many deposits (Hoeve and Sibbald, 1978) and the observation that graphite becomes increasingly degraded toward the ore zones in some deposits (Wang et al., 1989). The main objectives of this study are to determine the fluid composition, thermal conditions, fluid-structural relationships, and the role of graphite in the formation of the Phoenix deposit, through a combination of field (drill core) investigations, petrographic studies of altered and mineralized host rocks, microthermometric and microstructural studies of fluid inclusions, and petrographic and Raman spectroscopic studies of graphite.

Sampling and core description

In the summers of 2013 and 2014, a total of 120 samples were collected from 15 drill holes in the Wheeler River property, mostly from the Phoenix deposit (Fig. 2). Most of the drill cores examined are located on or near a NW-SE cross-section (Figs. 2 and 3), which is perpendicular to the regional structural trend in the area (Fig. 2). The drill cores were examined for lithological characteristics, with emphasis on fracture/vein fillings and associated alteration (Fig. 4). Ten oriented samples were collected for microstructural study.

Drill core samples from the basement are dominated by lower granulite facies metapelite to meta-psammopelite (Fig. 4A), containing graphite, garnet and/or cordierite. The metapelites are invaded by decimeter- to meter-thick foliation-parallel bodies of massive quartz (Fig. 4B) and spatially associated granitic pegmatite (Fig. 4C), which predate mineralization. In the graphitic metapelite unit, the amount of graphite appears to decrease toward the uranium orebody (Fig. 4D). Graphite is also locally concentrated in fractures cutting granitic pegmatite and associated quartz (Fig. 4E).

Samples from drill cores of the Athabasca Group overlying the unconformity are characterized by fragile, desilicified sandstone with interstitial clay alteration (Fig. 4F), with less developed intervals of relatively hard, silicified sandstone (Fig. 4G). Drusy quartz filled fractures and dissolution vugs are abundant in the Athabasca sandstone (Fig. 4H), and are locally developed in the basement as well (Fig. 4I). The abundance of drusy quartz near the mineralized zones is considered to be related to local silica oversaturation due to mineralization-related desilicification within the ore zones, and therefore it is considered to be syn- to post-mineralization.

Wang, K., Chi, G., Bethune, K.M., and Card, C.D., 2015. Fluid Composition, Thermal Conditions, Fluid-structural Relationships and Graphite Alteration of the Phoenix Uranium Deposit, Athabasca Basin, Saskatchewan, *in* Targeted Geoscience Initiative 4: unconformity-related uranium systems, (ed.) E.G. Potter and D.M. Wright; Geological Survey of Canada, Open File 7791, p. 93–102. doi:10.4095/295776

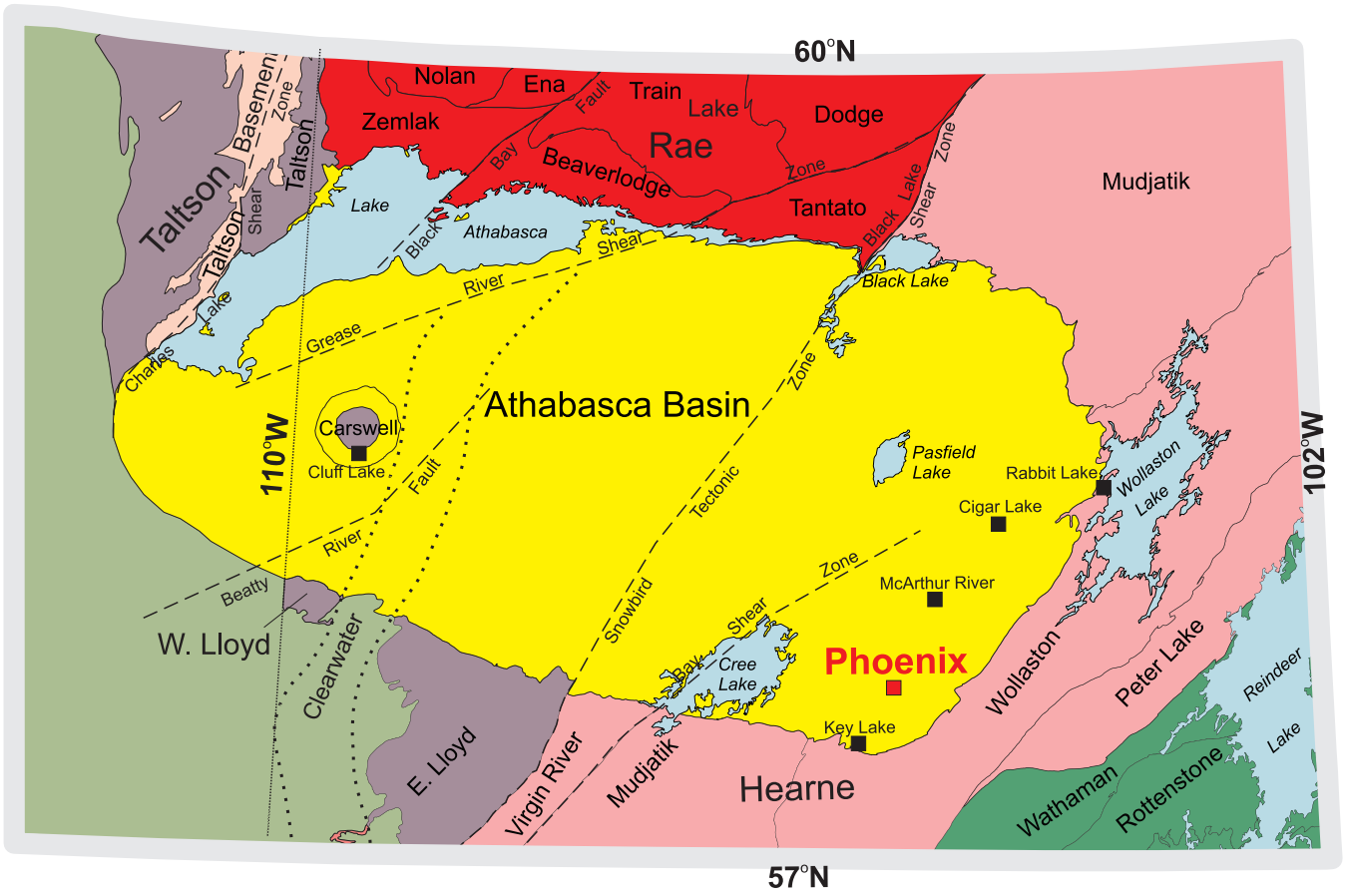

Figure 1. A regional geological map showing the location of the Phoenix uranium deposit in the southeastern part of the Athabasca Basin (modified from Card et al., 2007).

Analytical Methods

A hundred and one polished thin sections and seventy-six doubly polished thin sections were prepared for petrographic and fluid inclusion studies, respectively. The methods of fluid inclusion petrography, microthermometry, fluid inclusion plane (FIP) orientation measurement, and Raman spectroscopic study of graphite are described below.

Fluid inclusion petrography and microthermometry

Microthermometry was performed mainly on fluid inclusions distributed in growth zones of drusy quartz. The fluid inclusion assemblage (FIA) method (Goldstein and Reynolds, 1994) was used to evaluate the validity of microthermometric data. For spatially close fluid inclusions that cannot be strictly defined as FIAs, large variations in vapour percentage or homogenization temperature are still considered to indicate heterogeneous trapping or post-trapping modification (Chi and Lu, 2008). Microthermometry was carried out with a Linkam THMSG 600 heating/freezing stage in the Geofluids Laboratory at the University of Regina. The stage was calibrated with synthetic fluid inclusions of H_2O (ice-melting temperature = 0 °C; critical temperature = 374.1 °C) and H_2O-CO_2 (CO_2-melting temperature = -56.6 °C). The precision of the measured ice-melting temperature is ±0.2°C, and that for the homogenization temperature is ±2°C.

Fluid inclusion plane measurement

The orientations of FIPs (strike, dip direction, and dip angle) are measured from horizontally and vertically cut doubly polished sections with a conventional petrographic microscope, as described in Liu et al. (2011). The strike of the FIP is estimated by rotating the microscope stage to measure the angle between the strike of the FIP and the marked orientation on the section. The dip angle of the FIP was determined by changing the focus on different depths of the FIP as described below. First, the stage is rotated so that the FIP is oriented N-S, and focus is made on the upper part of the FIP. After recording the readings of the FIP on the horizontal crosshair (H_1) and the focusing screw (V_1), the focus is then changed to the lower part of the FIP, and new readings of both parameters (H_2, V_2) are recorded. The horizontal displacement of the focus of the FIP (ΔH) is equal to (H_2-H_1) multiplied by the length per unit for the objective used (e.g., for the x50 objective the length per unit is 2 mm). The vertical displacement of the focus of the FIP (ΔV) is equal to (V_2-V_1) multiplied by the depth per unit reading, which can be obtained by using a slide of known thickness. The dip angle (α) can then be calculated from the equation $\alpha = \tan^{-1}(\Delta V/\Delta H)$.

Raman spectrometry

Raman analysis was carried out with a Renishaw

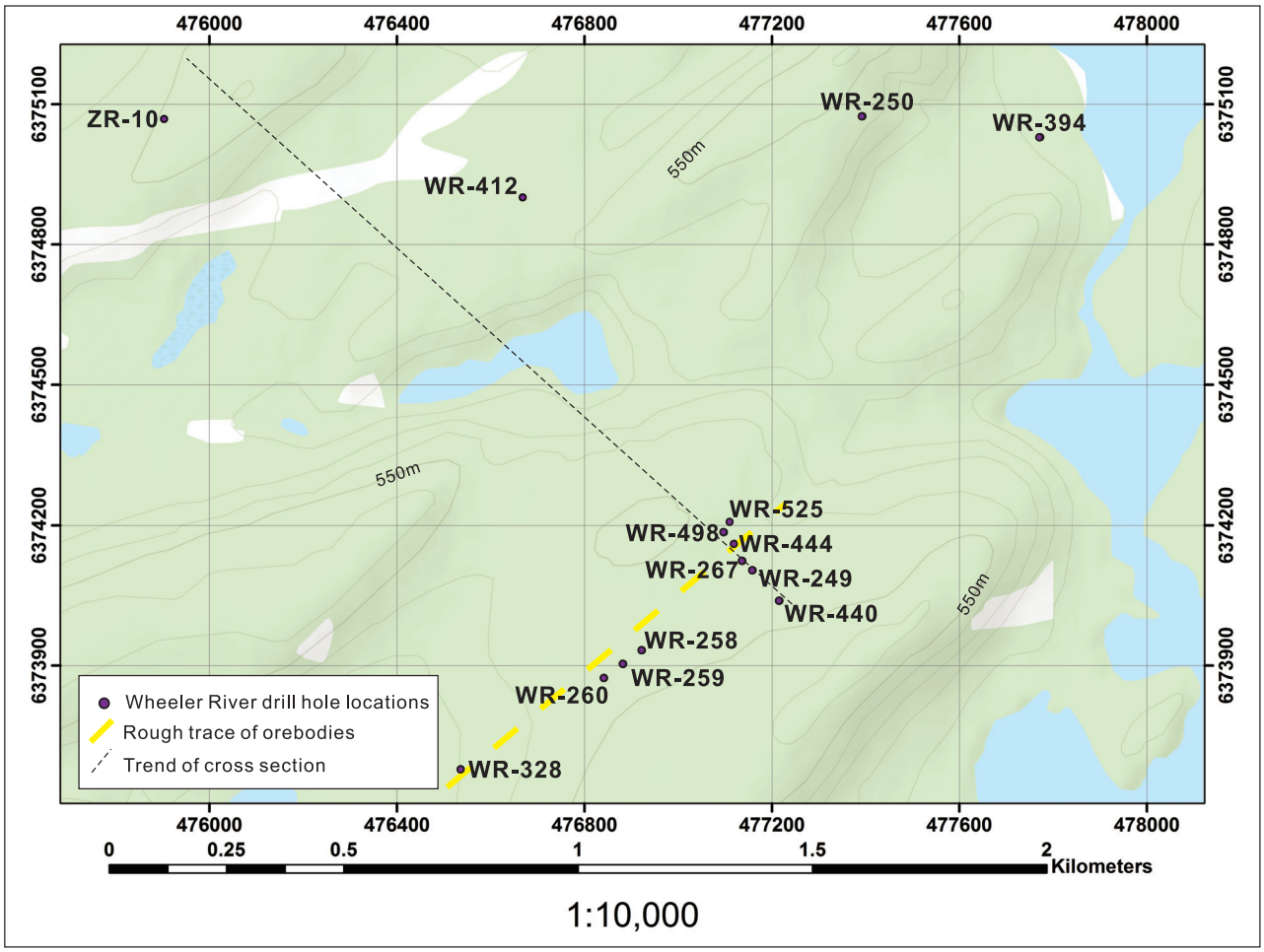

Figure 2. A map showing the locations of diamond drill holes studied from the Wheeler River area.

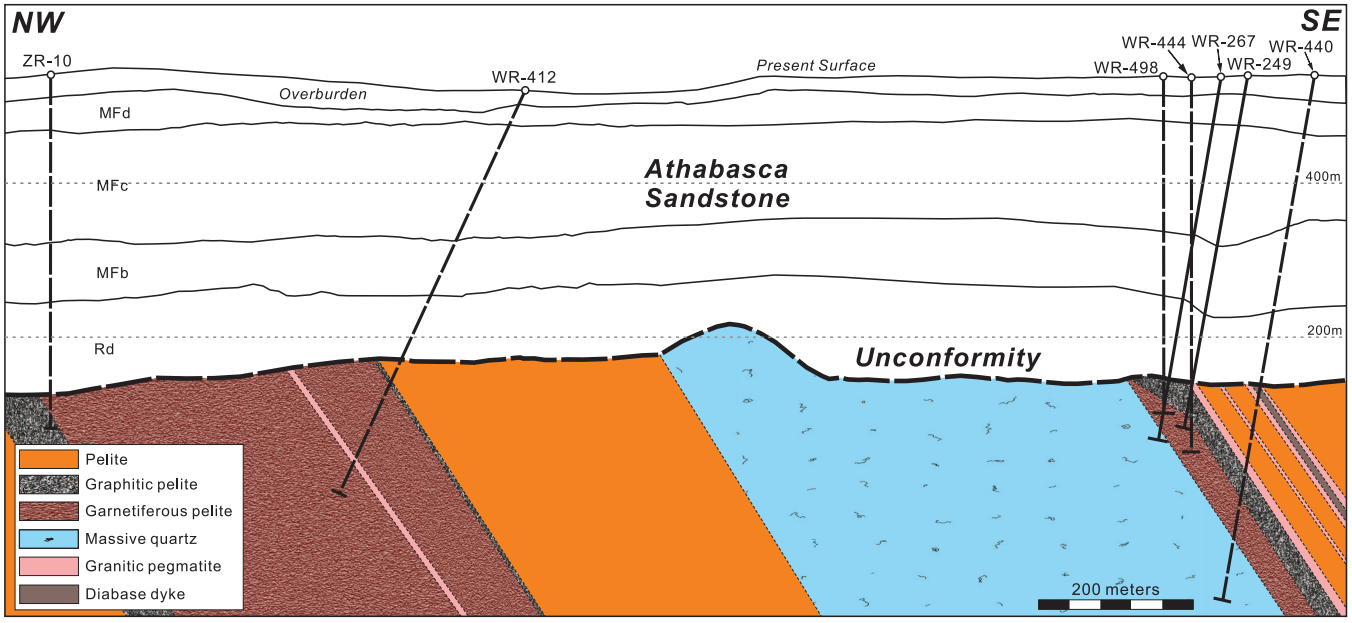

Figure 3. A schematic NW-SE cross section of the Phoenix deposit and neighboring area. Note only drill holes examined are shown (modified from Arseneau and Revering, 2010); the mineralization and the fault zones are not shown due to the limitation of the horizontal scale. Sandstone units: Rd = Read Formation, MF = Manitou Falls Formations: MFb = Bird Member, MFc = Collins Member, MFd = Dunlop Member.

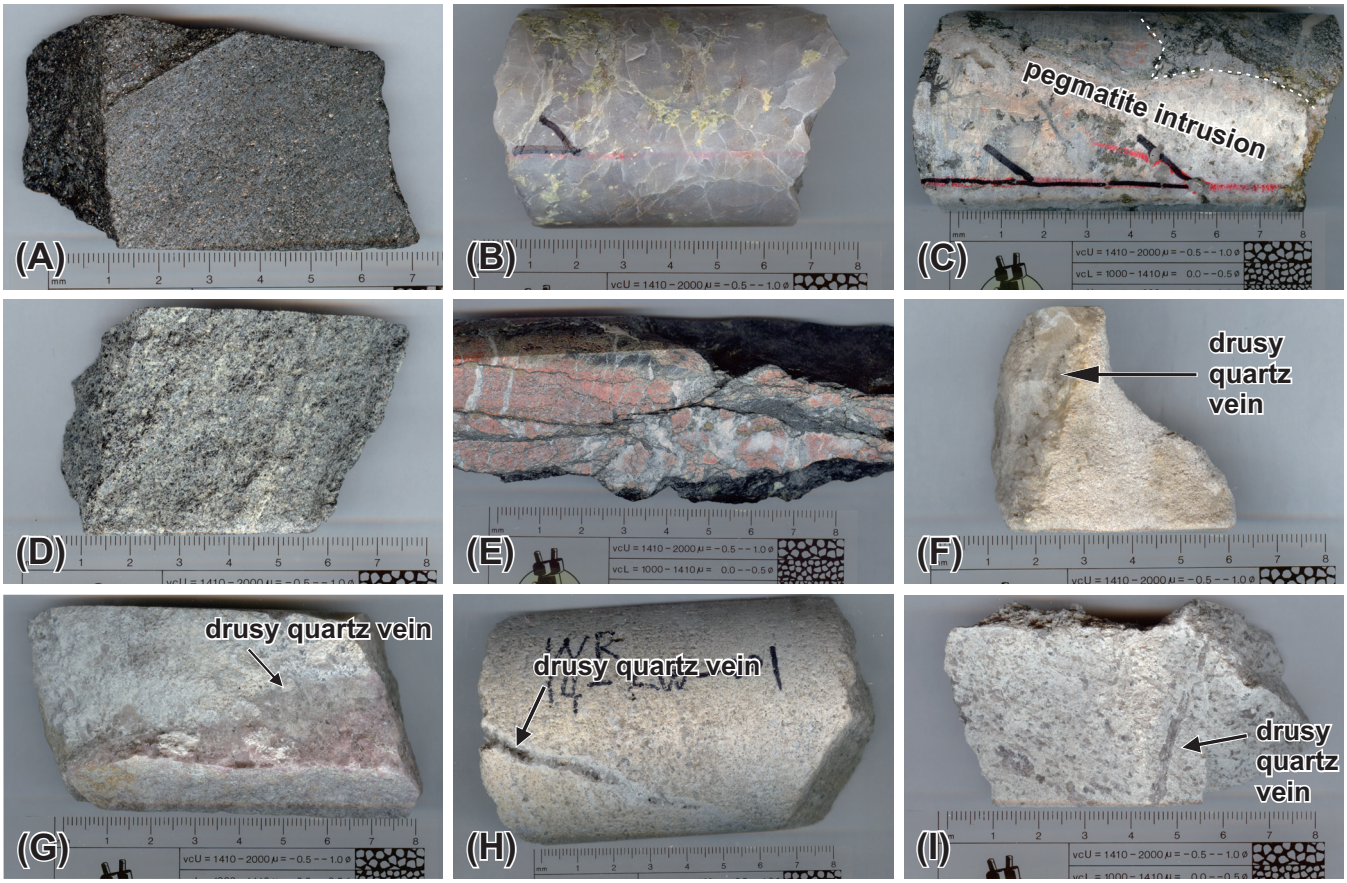

Figure 4. Photographs of drill core samples showing representative lithological units from the basement and the Athabasca Basin. A) Garnetiferous pelite with interstitial graphite (WR-440, 618.8m). B) Oriented sample of massive quartz (WR-440, 674m). C) Pegmatite intrusion cut by a calcite vein with minor quartz (WR-440, 479.6m). D) Weakly mineralized graphitic pelite (WR-328, 394.2m). E) Granitic pegmatite cut by black graphite-filled fractures (WR-440, 603m). F) Drusy quartz cutting intensely clay-altered sandstone (14-KW-046, WR-267). G) Drusy quartz cutting silicified sandstone (WR-328, 348.9m). H) Drusy quartz vein cutting weakly clay-altered sandstone (WR-525, 355.3m). I) Drusy quartz cutting strongly clay-altered granite (WR-560, 736m).

RM2000 laser Raman spectroscope at the Geofluids Laboratory of the University of Regina. The excitation laser wavelength is 514 nm, the grating is 1800, and the objective is x50 on the long working distance setting. For graphite analysis, as advised by Beyssac et al. (2003), the laser was focused on graphite below a contacting transparent mineral on the thin section surface, to avoid the polish defect typically developed on the surface of carbonaceous materials (Fig. 5). For each sample, six data points were analyzed, each with a 30-second acquisition time, in order to check the within-sample structural heterogeneity (Beyssac et al., 2002, 2003; Sadezky et al., 2005; Lahfid et al., 2010). We focused on the 1000–2000 cm^{-1} region, which includes all the first-order bands, and on 2000–3500 cm^{-1} for the second-order region (Beyssac et al., 2002, 2003; Sadezky et al., 2005; Lahfid et al., 2010).

Results

Petrographic and microthermometric study of fluid inclusions

Several types of aqueous fluid inclusions were identified in the drusy quartz from the sandstones above the unconformity, including: 1) biphase inclusions dominated by liquid with vapour percentage mainly from 5 to 13 % (Fig. 6A); 2) inclusions having a halite crystal at room temperature (Fig. 6B); 3) biphase inclusions with intermediate to very large vapour percentages (Fig. 6C); and 4) vapour-only inclusions (Fig. 6D). These inclusions occur randomly, as isolated inclusions or inclusion clusters, or along growth zones in the quartz (Fig. 6E). Based on the of FIA concept, fluid inclusions showing variable vapour percentages within a spatially close group (Fig. 6C.) are interpreted to have been heterogeneously entrapped, and only the inclusion with the lowest vapour percentage (hence homogenization temperature) is adopted (Goldstein and Reynolds, 1994; Chi and Lu, 2008). Therefore, most fluid inclusions examined are liquid-dominated biphase inclusions with a relatively consistent vapour percentage, with derived homogenization temperatures (T_h) mainly from 80 to 135 °C (L+V→L) (Fig. 7), ice-melting temperatures ranging from -23.6 to -33.6 °C, and corresponding salinities from 23.6 to 26.8 eq. wt. % NaCl, as calculated with the program of Chi and Ni (2007).

These T_h and salinity values (Fig. 7) are generally within the ranges reported for other unconformity-related uranium deposits and quartz overgrowths in the Athabasca Basin (e.g. Pagel et al., 1980; Kotzer and Kyser, 1995; Derome et al.,

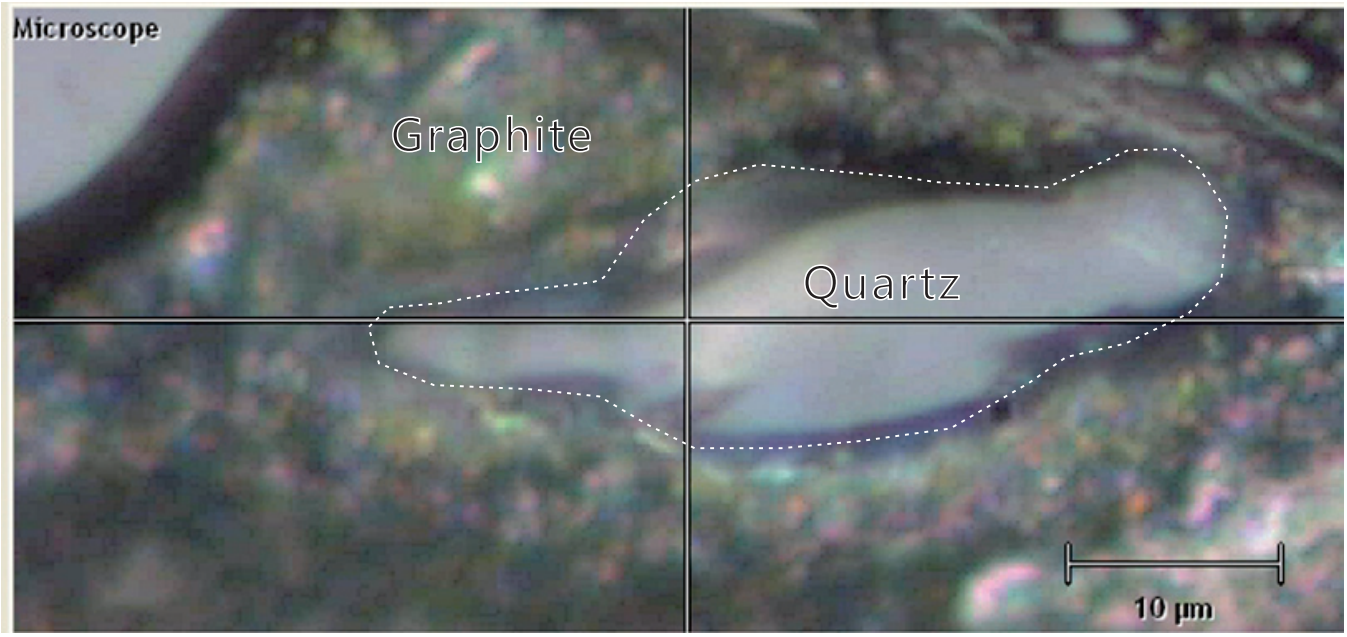

Figure 5. Photomicrograph showing a grain of quartz covering a graphite flake (14-KW-051).

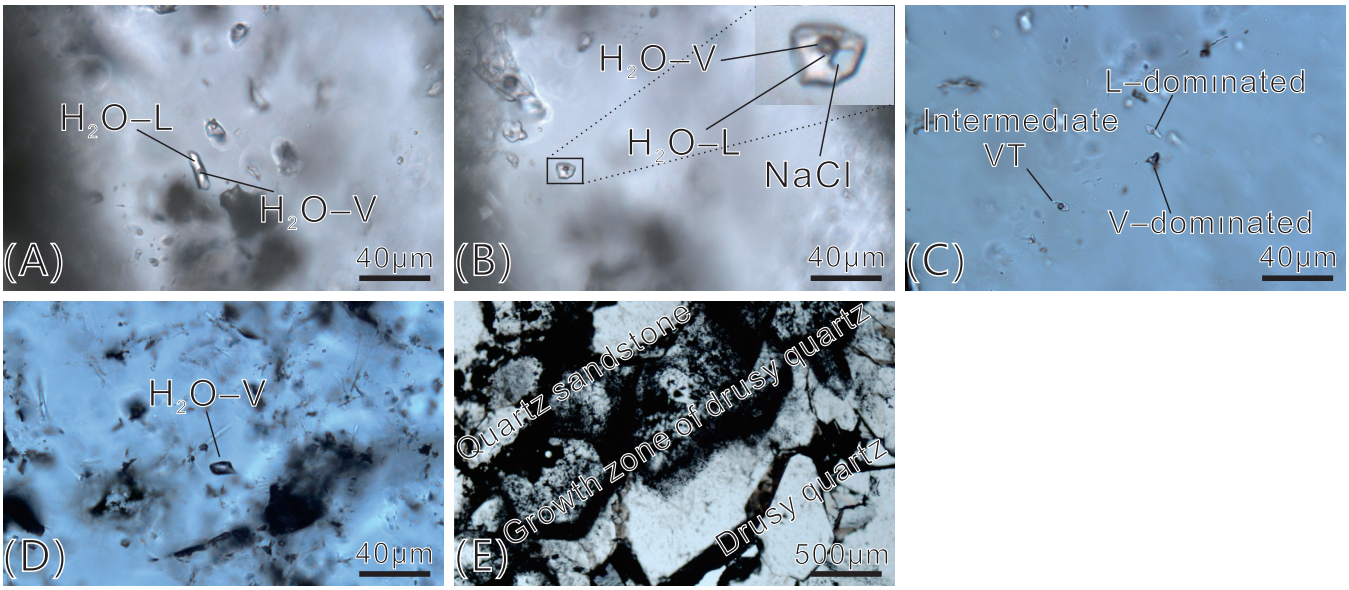

Figure 6. Microphotographs illustrating the types and occurrences of fluid inclusions in drusy quartz from the Manitou Falls Formation. A) Biphase aqueous fluid inclusions with relatively constant V/T ratios in a growth zone (WR-250, 341.8m). B) An isolated aqueous fluid inclusion with a halite cube (WR-250, 341.8m). C) A trail of fluid inclusions with variable V/T ratios (WR-328, 369.8m). D) A vapour-only inclusion (WR-328, 369.8m).

2005; Scott et al., 2011), although the T_h values are limited to the lower end of the spectrum. The abundance of vapour-only aqueous inclusions and their coexistence with biphase aqueous inclusions suggest boiling during the formation of the drusy quartz. This, together with the relatively low homogenization temperatures, indicates that the drusy quartz may have been formed during the waning stages of the uranium mineralization process, at lower pressures and temperatures than the main phase of mineralization.

Both aqueous and CO_2-dominated inclusions were found in the basement rocks. CO_2-dominated inclusions are well developed in densely distributed, parallel microfractures in the massive and pegmatoid quartz in the basement (Fig. 8A). These inclusions generally consist of three phases (vapour CO_2, liquid CO_2 and liquid water; Fig. 8B) or two phases (vapour CO_2 and liquid CO_2, without visible aqueous phase; Fig. 8C) at room temperature. Some biphase aqueous fluid inclusions with approximately 10 % of vapour also occur along the same microfractures as the CO_2-dominated fluid inclusions (Figs. 8B and C).

The CO_2-dominated inclusions in the basement were likely entrapped before the formation of the Athabasca Basin

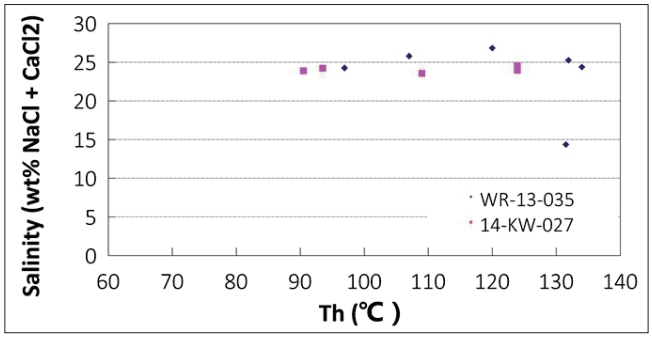

Figure 7. Homogenization temperature (T_h) versus salinity diagram for the studied aqueous inclusions (in WR-250, 341.8m and WR-328, 369.8m).

and uranium mineralization, probably in the retrograde metamorphic stage of Trans-Hudson orogenesis. Some of the microfractures formed at this stage may have been re-opened during the formation of the Athabasca Basin, facilitating circulation of basinal brines into the basement. Mercadier et al. (2010) provided evidence of such re-activation of pre-existing fractures in basement rocks, with infiltration of basinal brines, proximal to the P-Patch deposit along the southern margin of the basin.

Microstructural study of fluid inclusion planes

The orientations of (FIP) were measured for an oriented sample of a dolomite-quartz vein cutting graphitic metapelite in the basement (Fig. 9A, WR-440, 604.1m). Two main sets of subvertical FIPs were observed in the euhedral quartz from the vein in a horizontally-cut oriented thin section (Fig. 9B): one striking 190–210° and the other striking 90–110° (Fig. 9C). One set is long and is perpendicular or sub-perpendicular to the foliation of the host rock, whereas the other set is relatively short and is parallel or sub-parallel to the foliation. Mutual crosscutting relationships are not evident in this thin section, therefore the relative timing of the two sets remains uncertain. Vertically-cut oriented thin sections from the same drill core also show that subvertical FIPs are dominant (Fig. 10), indicating that the data obtained from the horizontally-cut thin section are not biased. The fluid inclusions entrapped in the FIPs in the horizontally-cut thin section were generally too small to conduct microthermometric measurements.

The FIPs are interpreted as simple Mode I extension fractures, therefore the pole to an FIP corresponds to the minimum principal stress (σ3) direction of the stress field (Lespinasse and Pecher, 1986; Lespinasse, 1999). Accord-

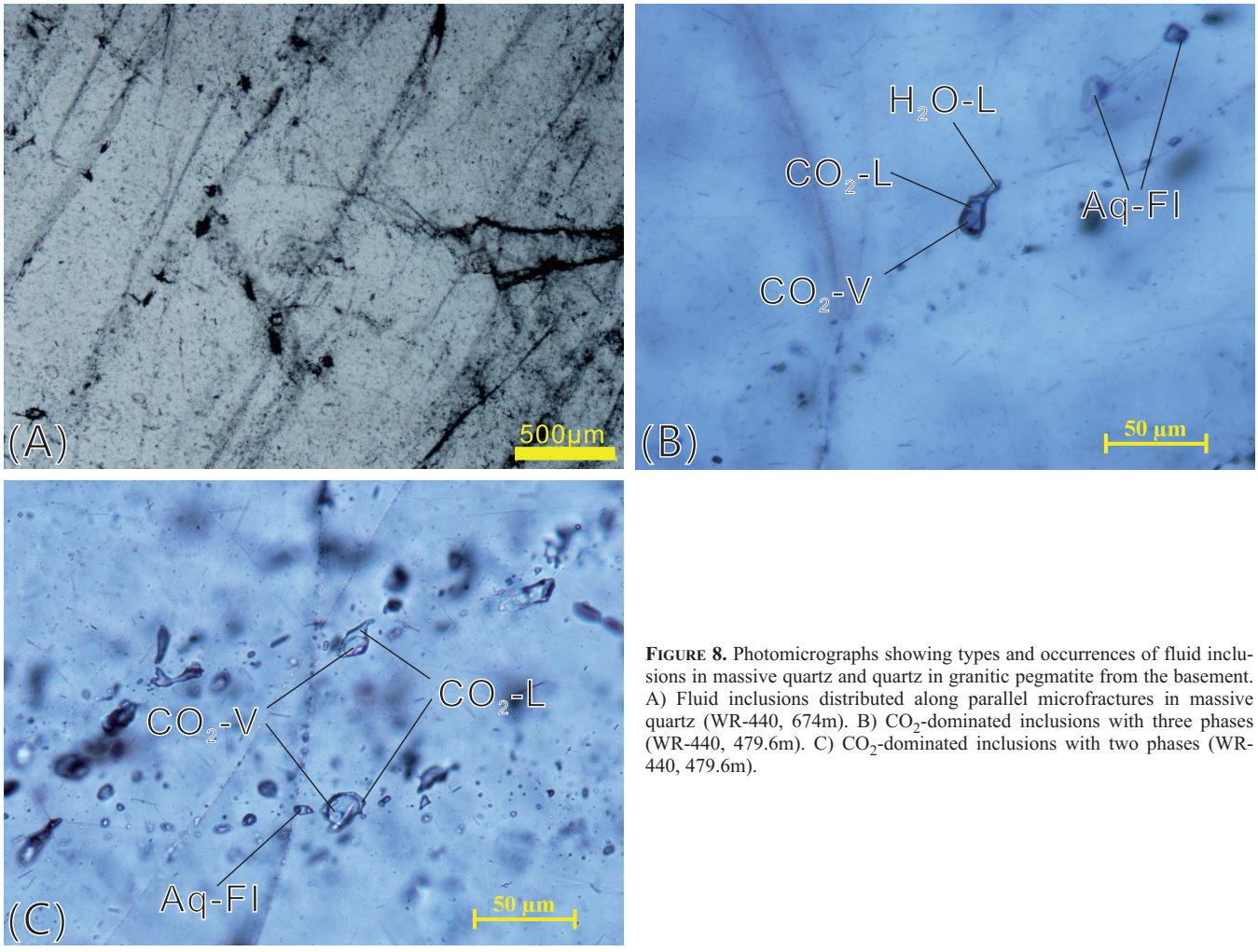

Figure 8. Photomicrographs showing types and occurrences of fluid inclusions in massive quartz and quartz in granitic pegmatite from the basement. A) Fluid inclusions distributed along parallel microfractures in massive quartz (WR-440, 674m). B) CO_2-dominated inclusions with three phases (WR-440, 479.6m). C) CO_2-dominated inclusions with two phases (WR-440, 479.6m).

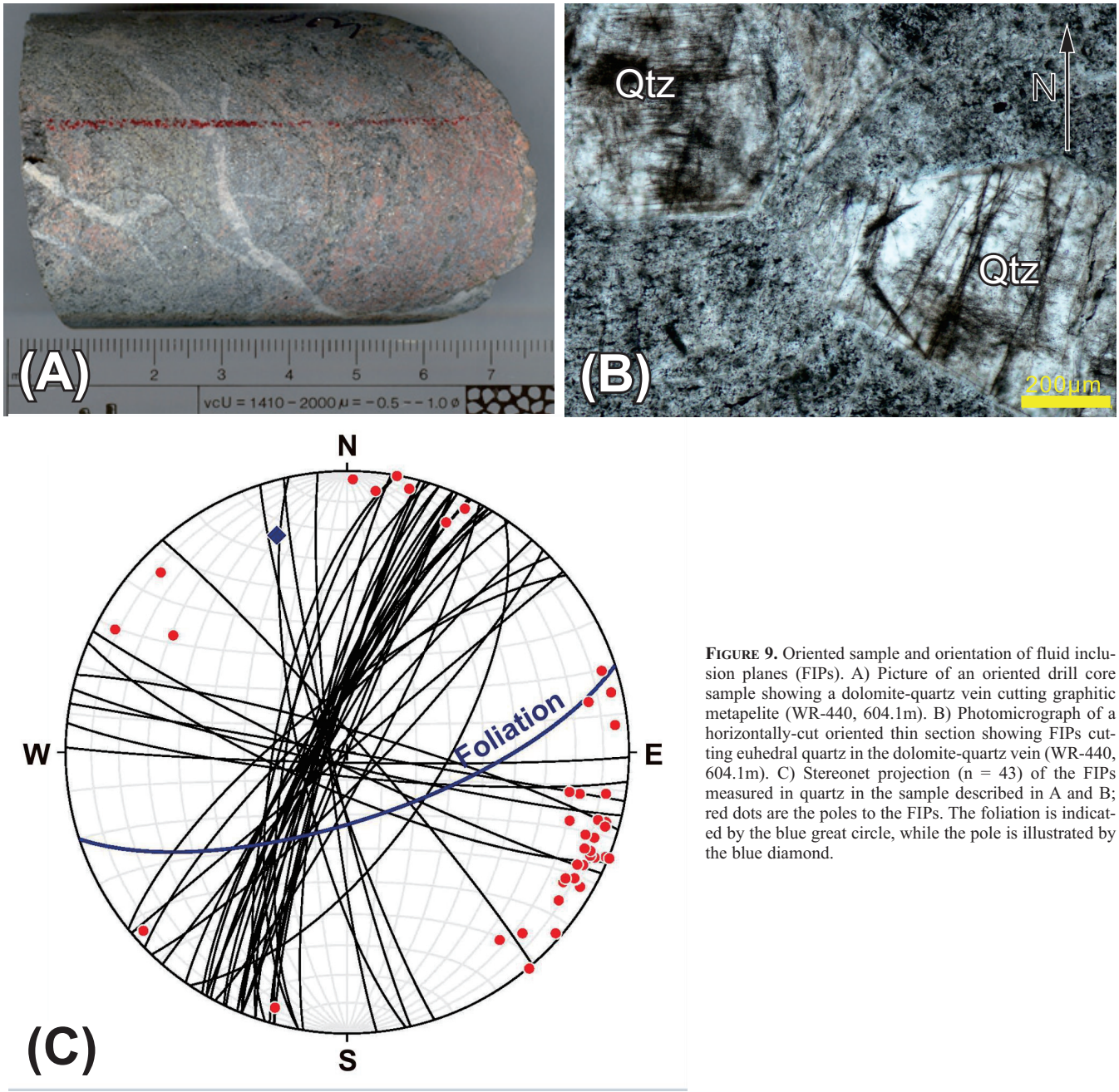

Figure 9. Oriented sample and orientation of fluid inclusion planes (FIPs). A) Picture of an oriented drill core sample showing a dolomite-quartz vein cutting graphitic metapelite (WR-440, 604.1m). B) Photomicrograph of a horizontally-cut oriented thin section showing FIPs cutting euhedral quartz in the dolomite-quartz vein (WR-440, 604.1m). C) Stereonet projection (n = 43) of the FIPs measured in quartz in the sample described in A and B; red dots are the poles to the FIPs. The foliation is indicated by the blue great circle, while the pole is illustrated by the blue diamond.

ingly, the two main directions of FIPs discussed above are considered to be related to two different stress fields, one stage with the σ3 direction trending WNW- ESE and another stage with σ3 direction trending NNW- SSE. It remains to be determined whether the maximum principal stress (σ1) and intermediate principal stress (σ2) also switched between horizontal and vertical directions. If σ1 was vertical, both σ2 and σ3 must have been horizontal, and the FIPs formed in the vertical plane. However, subvertical FIPs could still have formed if σ1 was horizontal but in that case one cannot discriminate if σ2 or σ3 was the vertical stress. In short, the dominance of subvertical FIPs may indicate an extensional stress field (σ1 vertical), but the possibility of a compressional stress field (σ1 horizontal) cannot be ruled out.

Petrographic and Raman spectroscopic study of graphite

A suite of samples of graphitic metapelite were collected from the alteration zones hosting the uranium mineralization near the unconformity down to the relatively unaltered basement in drill core of WR-267. Three samples have been selected with increasing distance from the lower boundary of the major uranium concentration: 14-KW-048 (5 m), 14-KW-051 (15 m), 14-KW-053 (25 m). The graphite in the samples was examined with a petrographic microscope and a Raman spectrometer.

Petrographic observations of graphite indicate that the graphite closer to the uranium mineralization has more jagged grain boundaries than that further from the uranium mineralization (Fig. 11).

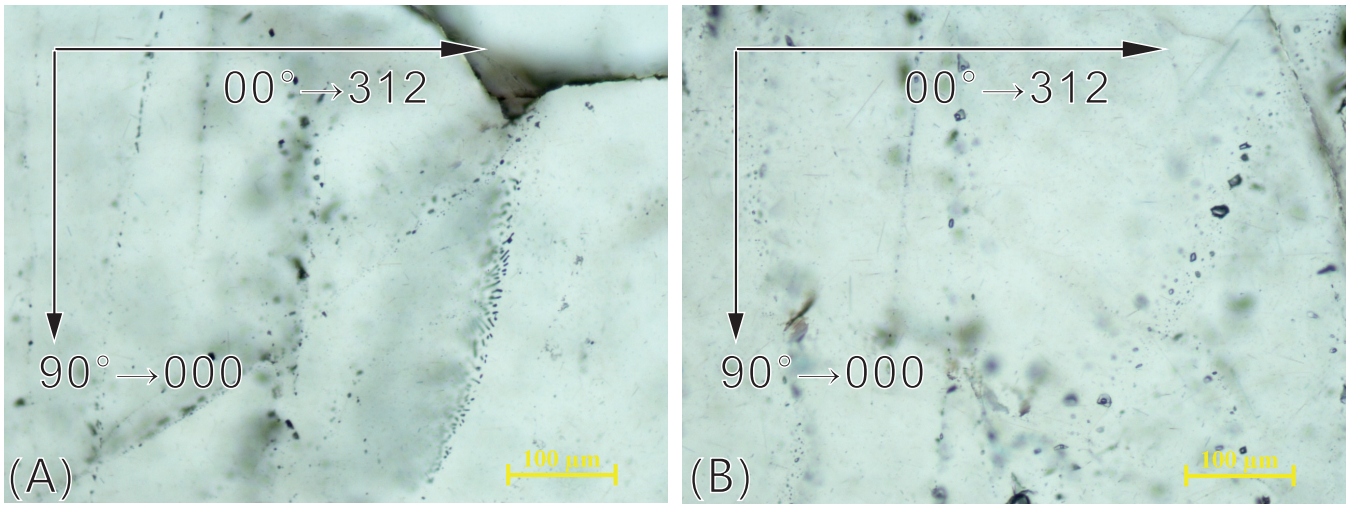

Figure 10. Photomicrographs of vertically-cut oriented thin sections showing the dominance of subvertical FIPs in pegmatoid quartz from a pegmatite vein (WR-440, 479.6m). Note the FIPs comprise CO_2-dominated fluid inclusions, biphase aqueous inclusions and monophase aqueous inclusions.

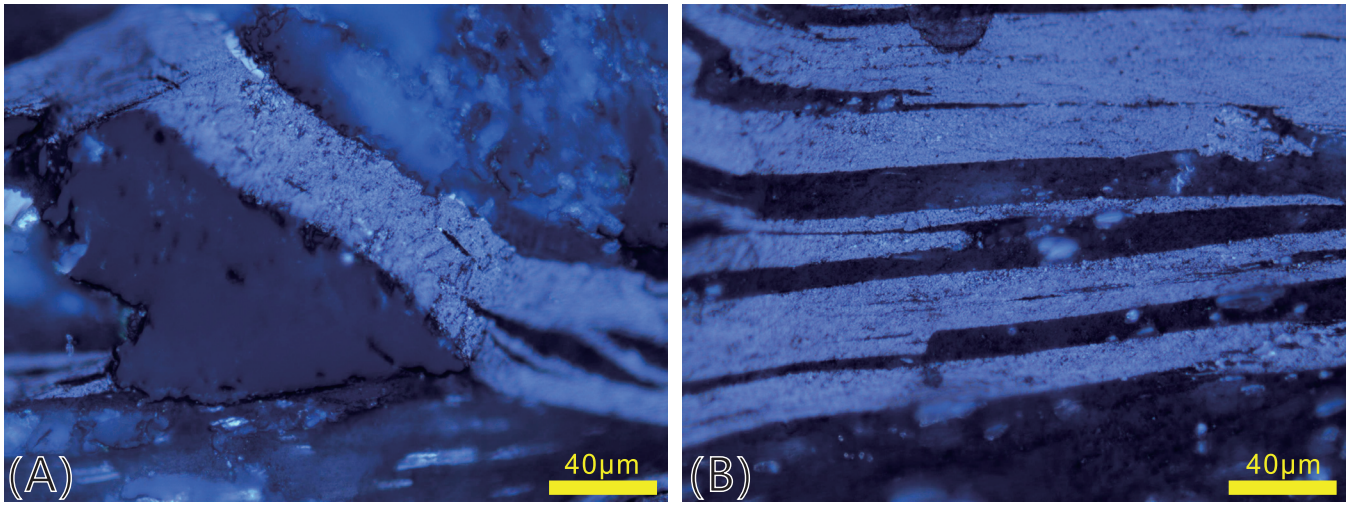

Figure 11. Photomicrographs showing graphite in reflected light: A) in metapelite 5m from orebody (WR-267, 414.1m); and B) in metapelite 25m from orebody (WR-267, 433m).

The Raman spectra of the three samples located at different distances from the mineralized zone, as described above, are shown in Figure 12. All of the spectra show a prominent G band (~1583 cm^{-1}) in the first-order region (Fig. 12A), indicative of well-crystallized graphite (Beyssac et al., 2002, 2003; Sadezky et al., 2005; Lahfid et al., 2010). However, graphite in sample 14-KW-048 (red), which is closest to the mineralization zone, appears to have more obvious D1 and D2 bands (~1367 cm^{-1} and 1609 cm^{-1}), which are related to defects in graphite (Beyssac et al., 2002). In contrast, the spectrum of the sample furthest from the mineralization zone, 14-KW-053 (blue; Fig. 12A), shows almost no additional bands to the G band. The spectra in the second-order region are similar among the three samples (Fig. 12B), although 14-KW-048 appears to have a higher contribution of S2 bands than other samples.

Although some studies suggested that graphitization is an irreversible process (Beyssac et al., 2002), a gradual loss of the structural ordering of graphite toward some uranium deposits in the Athabasca Basin has been demonstrated by Wang et al. (1989) and Pascal et al. (2015). In this study, the higher D1 and S2 intensities of the sample closest to the mineralization zone than those away from it, as described above, also suggest that the graphite near the mineralization is relatively disordered.

Summary and implications for exploration

Collectively, the field and petrographic observations, coupled with preliminary fluid inclusion analysis, support previous studies (e.g. Jefferson et al., 2007 and references therein) that noted different structural regimes and fluid systems were developed in the pre-Athabasca stage versus the syn- to post-Athabasca, uranium mineralization stages. The pre-Athabasca stage was characterized by ductile deformation as demonstrated by the development of foliation, followed by pegmatization, massive silicification, and circula-

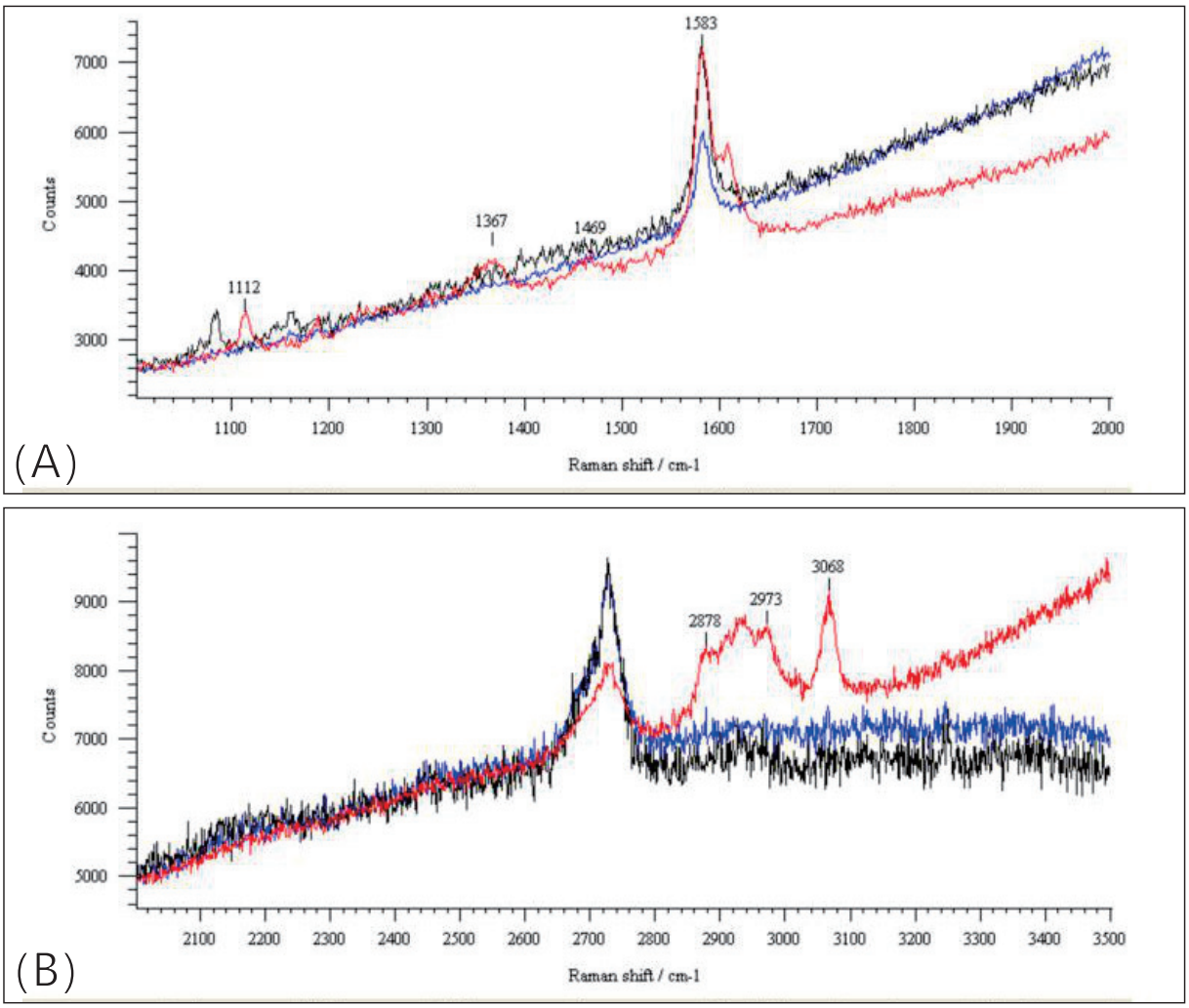

Figure 12. Representative Raman spectra of graphite of three samples with different distances from the ore zone. A) In the first-order region; Red: 14-KW-048, 5m from ore zone; Black: 14-KW-051, 15m from the ore zone; and Blue: 14-KW-053, 25m from the ore zone. B) In the second order region; Red: 14-KW-048, 5m from ore zone; Black: 14-KW-051, 15m from ore zone; and Blue: 14-KW-053, 25m from the ore zone.

tion of metamorphic fluids in a relatively high *P–T* environment, as indicated by the abundance of CO_2-bearing fluid inclusions. In contrast, the syn- to post-Athabasca stages were characterized by brittle deformation, as reflected by the development of fractures filled by drusy quartz in the basal Athabasca Group and the uppermost part of the basement, and by circulation of basinal brines in a relatively low *P–T* environment, as recorded by the aqueous fluid inclusions in the drusy quartz. Furthermore, the fluid may have experienced boiling at this stage, as indicated by the coexistence of vapour-only and biphase aqueous inclusions, again pointing to a relatively low *P* environment. Fluid boiling has been recognized in many other Proterozoic uranium deposits in northern Canada (Chi et al., 2014), and its significance for uranium mineralization is the subject of several on-going studies, including this one. It remains to be investigated whether the low fluid pressure that appears to have instigated boiling was caused by faulting, i.e. through the fault-valve or seismic pumping mechanisms (Sibson et al., 1988; Sibson, 1994), or was related to a shallow, epithermal environment. These structural-fluid relationships and associated geochemical signatures are potentially important for uranium exploration.

Preliminary FIP orientation studies indicate that subvertical microfractures are developed in the basement rocks, likely after the ductile deformation stage. These microfractures, dominantly subvertical, suggest that the local stress field in the Phoenix deposit may have been extensional at certain periods of time in the post-Athabasca, brittle deformation stage, although the subvertical FIPs may also have formed in a compressional regime.

The close spatial relationship between uranium mineralization and graphitic units in the basement in the Phoenix deposit, as also observed in many other unconformity-related uranium deposits, suggests that graphite played a role in uranium mineralization. However, its exact role remains unclear — was it directly involved in reducing U^{6+} in the fluids, or was it the precursor to hydrocarbons that acted as the reductants for uraninite precipitation? More work on fluid inclusion composition, especially the volatile components, is

being conducted to address this question. Preliminary Raman spectroscopic studies of graphite samples from different localities suggest that the graphite becomes increasingly disordered toward the ore zone. This trend, if confirmed by further studies (ongoing), could be used as an indicator of mineralization.

Acknowledgments

Funding for this research was provided by the Targeted Geoscience Initiative 4 (TGI-4) uranium ore systems project, through a grant to K.M. Bethune and G. Chi, and in part by a NSERC-Discovery grant (to G. Chi). Logistical support from Denison Mines Corp., and assistance from Clark Gamelin, Yongxing Liu, Zenghua Li and Morteza Rabiei during the field work are gratefully acknowledged. The paper has benefited from the review by Antonin Richard and detailed review and editing of Eric Potter.

References

Arseneau, G., and Revering, C., 2010. Technical report on the Phoenix deposit (Zones A & B) - Wheeler River project, eastern Athabasca Basin, Northern Saskatchewan, Canada; NI 43-101 technical report prepared for Denison Mines Corp., by SRK Consulting, 95 p.

Beyssac, O., Goffé, B., Chopin, C., and Rouzaud, J.-N., 2002. Raman spectra of carbonaceous material in metasediments: a new geothermometer; Metamorphic Geology, v. 20, p. 859–871.

Beyssac, O., Goffé, B., Petitet, J.P., Froigneux, E., and Rouzaud, J.-N., 2003. On the characterization of disordered and heterogeneous carbonaceous materials using Raman spectroscopy; Spectrochimica Acta Part A, v. 59, p. 2267–2276.

Card, C., Pana, D., Portella, P, Thomas, D.J., and Annesley, I.R., 2007. Basement rocks of the Athabasca Basin, Saskatchewan and Alberta; in EXTECH IV: Geology and Uranium EXploration TECHnology of the Proterozoic Athabasca Basin, Saskatchewan and Alberta, (ed.) C.W. Jefferson and G. Delaney; Geological Survey of Canada, Bulletin 588, p. 69–87.

Chi, G., and Ni, P., 2007. Equations for calculation of NaCl/(NaCl+$CaCl_2$) ratios and salinities from hydrohalite-melting and ice-melting temperatures in the H_2O-NaCl-$CaCl_2$ system; Acta Petrologica Sinica, v. 23, p. 33–37.

Chi, G., Liang, R., Ashton, K., Haid, T., Quirt, D., Fayek, M. 2014. Evidence of fluid immiscibility from uranium deposits in northern Saskatchewan and Nunavut and potential relationship with uranium precipitation; 2014 GAC-MAC Annual Conference, Program with Abstracts, v. 37, p. 57.

Chi, G. and Lu, H. 2008. Validation and representation of fluid inclusion microthermometric data using the fluid inclusion assemblage (FIA) concept; Acta Petrologica Sinica, v. 24, p. 1945–1953.

Dann, J., Hattori, K., Potter, E.G., and Sorba, C., 2013. Discrimination of elemental assemblages in the alteration halo of the Phoenix deposit, Saskatchewan, through applied GIS; Geological Survey of Canada, Open File 7463. doi:10.4095/293122

Derome, D., Cathelineau, M., Cuney, M., Fabre, C., Lhomme, T., and Banks, D. A., 2005. Mixing of sodic and calcic brines and uranium deposition at McArthur River, Saskatchewan, Canada: A Raman and laser-induced breakdown spectroscopic study of fluid inclusions; Economic Geology, v. 100, p. 1529–1545.

Gamelin, C., Sorba, C., and Kerr, W., 2010. The discovery of the Phoenix Deposit: A new high-grade Athabasca Basin unconformity-type uranium deposit, Saskatchewan, Canada; Saskatchewan Geological Survey Open House, 2010 Abstract Volume, p. 17.

Goldstein, R.H. and Reynolds, T.J. 1994. Systematics of fluid inclusions in diagenetic minerals; SEPM Short Course, v. 31, 199 p.

Hoeve, J., and Sibbald, T.I., 1978. On the genesis of Rabbit Lake and other unconformity-type uranium deposits in northern Saskatchewan, Canada; Economic Geology, v. 73, p. 1450–1473.

Jefferson, C.W., Thomas, D.J., Gandhi, S.S., Ramaekers, P., Delaney, G., Brisbin, D., Cutts, C., Portella, P. and Olson, R.A., 2007. Unconformity-associated uranium deposits of the Athabasca basin, Saskatchewan and Alberta; in EXTECH IV: Geology and Uranium EXploration TECHnology of the Proterozoic Athabasca Basin, Saskatchewan and Alberta, (ed.) C.W. Jefferson and G. Delaney; Geological Survey of Canada, Bulletin 588, p. 23–67.

Kerr, W.C., 2010. The discovery of the Phoenix deposit: a new high-grade Athabasca Basin unconformity-type uranium deposit, Saskatchewan, Canada; in The Challenge of Finding New Mineral Resources: Global Metallogeny, Innovative Exploration, and New Discoveries, Volume II: Zinc-Lead, Nickel-Copper-PGE, and Uranium, (ed.) R.J. Goldfarb, E.E. Marsh and T. Monecke; Society of Economic Geologists, p. 703–725.

Kotzer, T., Kyser, T., 1995. Petrogenesis of the Proterozoic Athabasca Basin, northern Saskatchewan, Canada, and its relation to diagenesis, hydrothermal uranium mineralization and paleohydrogeology; Chemical Geology, v. 120, p.45–89.

Lahfid, A., Beyssac, O., Deville, E., Negro, F., Choppin, C., and Goffé, B., 2010. Evolution of the Raman spectrum of carbonaceous material in low-grade metasediments of Glarus Alps (Switzerland); Terra Nova, v. 22, p. 354–360.

Lespinasse, M., Pecher, A., 1986. Microfracturing and regional stress field: a study of preferred orientations of fluid inclusion planes in a granite from the Massif Central, France; Journal of Structural Geology, v. 8, p. 169–180.

Lespinasse, M., 1999. Are fluid inclusion planes useful in structural geology?; Journal of Structural Geology, v. 21, p.1237–1243.

Liu, Y., Chi, G., Bethune, K.M., and Dube, B., 2011. Fluid dynamics and fluid-structural relationships in the Red Lake mine trend, Red Lake greenstone belt, Ontario, Canada; Geofluids, v. 11, p. 260–279.

Mercadier, J., Richard, A., Boiron, M.C., Cathelineau, M., Cuney, M., 2010. Migration of brines in the basement rocks of the Athabasca Basin through microfracture networks (P-Patch U deposit, Canada); Lithos, v. 115, p. 121–136.

Pagel, M., Poty, B., Sheppard, S.M.F., 1980. Contribution to some Saskatchewan uranium deposits mainly from fluid inclusion and isotopic data; in International Uranium Symposium on the Pine Creek Geosyncline, International Atomic Energy Agency, Vienna, p. 639–654.

Pascal, M., Ansdell, K.M., and Annesley, I.R., 2015. Graphite-bearing and graphite-depleted basement rocks in the Dufferin Lake zone, south-central Athabasca Basin, Saskatchewan; *in* Targeted Geoscience Initiative 4: unconformity-related uranium systems, (ed.) E.G. Potter and D.M. Wright; Geological Survey of Canada, Open File 7791, p. 83-92. doi:10.4095/295776

Power, M.J., Hattori, K., Sorba, C., and Potter, E.G., 2012. Geochemical anomalies in the soil and uppermost siliciclastic units overlying the Phoenix uranium deposit, Athabasca Basin, Saskatchewan; Geological Survey of Canada, Open File 7257, 36 p. doi:10.4095/291981

Sadezky, A., Muckenhuber, H., Grothe, H., Niessner, R., and Pöschl, U., 2005. Raman microspectroscopy of soot and related carbonaceous materials: spectral analysis and structural information; Carbon, v. 43, p. 1731–1742.

Scott, R., Chi, G., and Bosman, S., 2011. A petrographic and fluid inclusion study of the Athabasca Group sandstones from the Rumpel Lake drill core, Athabasca Basin, Northern Saskatchewan; in Summary of Investigations 2011, volume 2, Saskatchewan Geological Survey, Miscellaneous Report 2011-4.2, Paper A5, 10 p.

Sibson, R.H., 1994. Crustal stress, faulting and fluid flow; Geological Society Special Publications, v. 78, p. 69–84.

Sibson, R.H, Robert, F., and Poulsen, K.H., 1988. High angle reverse faults, fluid pressure cycling, and mesothermal gold-quartz deposits; Geology, v. 16, p. 551–555.

Wang, A., Dhamelincourt, P., Dubessy, J., Guerard, D., Landais, P., and Lelaurain, M., 1989. Characterization of graphite alteration in an uranium deposit by micro-Raman spectroscopy, X-Ray diffraction, transmission electron microscopy and scanning electron microscopy; Carbon, v. 27, p. 209–218.